Membrane fusion during phage lysis

Manoj Rajaure[a], Joel Berry[b], Rohit Kongari[a], Jesse Cahill[a], and Ry Young[a,1]

[a]Center for Phage Technology, Department of Biochemistry and Biophysics, Texas A&M University, College Station, TX 77843-2128; and [b]Department of Microbiology, Pasteur Institute, 75724 Paris, France

Edited by Thomas J. Silhavy, Princeton University, Princeton, NJ, and approved March 18, 2015 (received for review October 29, 2014)

In general, phages cause lysis of the bacterial host to effect release of the progeny virions. Until recently, it was thought that degradation of the peptidoglycan (PG) was necessary and sufficient for osmotic bursting of the cell. Recently, we have shown that in Gram-negative hosts, phage lysis also requires the disruption of the outer membrane (OM). This is accomplished by spanins, which are phage-encoded proteins that connect the cytoplasmic membrane (inner membrane, IM) and the OM. The mechanism by which the spanins destroy the OM is unknown. Here we show that the spanins of the paradigm coliphage lambda mediate efficient membrane fusion. This supports the notion that the last step of lysis is the fusion of the IM and OM. Moreover, data are provided indicating that spanin-mediated fusion is regulated by the meshwork of the PG, thus coupling fusion to murein degradation by the phage endolysin. Because endolysin function requires the formation of μm-scale holes by the phage holin, the lysis pathway is seen to require dramatic dynamics on the part of the OM and IM, as well as destruction of the PG.

spanin | membrane fusion | spheroplast | holin | endolysin

Phage lysis, the most common cytolytic event in the biosphere, has been extensively studied in phage λ, where four genes encoding five proteins (Fig. 1*A*) effect a three-step lytic process that releases the progeny virions (1, 2). The infection cycle suddenly terminates when the S105 holins, small membrane proteins encoded by gene *S*, are redistributed into large 2D foci, resulting in the formation of μm-scale holes in the cytoplasmic membrane (3). This event, called holin "triggering," occurs at a time specific to the allelic state of *S* and is temporally regulated by the proportion of a second *S* product, the antiholin S107 (4, 5). The R endolysin is then able to escape through the holes to attack the peptidoglycan (PG). Because the PG layer confers shape and mechanical integrity to the cell, holin and endolysin function was long thought to be necessary and sufficient for lysis (6, 7). However, recent genetic and physiological studies revealed that two other λ proteins, Rz and Rz1, are also required (Fig. 1*B*) (8). Rz and Rz1 are a type II integral membrane protein (*N*-in, C-out) and an outer membrane (OM) lipoprotein, respectively (9–11). Interacting by the C-termini of their periplasmic domains, Rz and Rz1 form a complex spanning the entire periplasm, designated as the spanin complex to denote its topology in the envelope. Accordingly, Rz and Rz1 are designated as the inner membrane (IM) (i-spanin) and OM (o-spanin) subunits of the spanin complex (Fig. 1 *A* and *B*) (12). Experiments with GFP-Rz chimeras and biochemical analysis of envelope proteins indicate that the spanin complexes accumulate in the envelope throughout the morphogenesis period of the infection cycle (8, 13). The available data indicate that, after destruction of the PG by the endolysin, the spanin complex functions to disrupt the OM. In the absence of spanin function, the infection cycle terminates in a spherical cell form, in which the IM has been lethally permeabilized by the holin, the PG has been destroyed by the endolysin, but the OM is intact (Fig. 1*C*, previously published in ref. 8).

The λ *Rz* i-spanin and *Rz1* o-spanin genes have a unique genetic architecture, with the latter entirely contained within the former in the +1 reading frame (Fig. 1*A*); these are the only genes in biology that share the same DNA in different reading frames and are both required for the same biological function (14). Secondary structure analysis of Rz indicates that its periplasmic domain has a mostly alpha-helical structure, with two helical domains separated by a central unstructured hinge region. In contrast, the mature Rz1 o-spanin is only 40 aa and is predicted to be unstructured, largely because of its high proportion of proline residues (10 of 40). These predictions were supported by CD analysis of the purified periplasmic domains (13). When mixed, the two periplasmic domains formed complexes with a 1:1 subunit ratio and underwent a conformational change involving a dramatic increase in alpha-helicity. Imaged by negative-stain EM, the complexes were found to be oligomeric rod-like bundles of ∼25 nm in length, corresponding to the measured width of the lateral periplasm. The complexes are thought to form by interactions at the C termini of both the subunits, a notion supported by yeast two-hybrid analysis of the analogous i-spanin and o-spanin genes of phage T7 (15).

The fundamental question is how the Rz–Rz1 complex achieves disruption of the OM barrier. It was proposed that spanin complexes interacted with holins to transduce the μm-scale lesions formed in the cytoplasmic membrane directly to the OM (16). However, Berry et al. (2) showed that spanin function was also required for lysis even if the endolysin was secreted via the general secretory pathway, rather than via the holin-mediated holes. Thus, spanin function is necessary for lysis after degradation of the murein layer, irrespective of the presence of holin lesions in the cytoplasmic membrane. We have proposed that spanins remove the OM as a topological barrier by fusing it with the cytoplasmic membrane (2). Indeed, membrane fusogenic activity has been reported for Rz1 and suggested as a component of lambda lysis, based on studies with purified protein and overexpression of Rz1 in vivo (17). However, these results have been challenged (2).

Here we report experiments designed to interrogate the lytic mechanism of the phage spanins. The results are discussed in terms of the membrane fusion model, the regulation of spanin function, and the potential for leveraging spanins for the study of the fundamental process of membrane fusion.

Significance

These findings reveal that membrane fusion is integral to the most common prokaryotic cell fate, phage lysis, and constitutes an unprecedented topological mechanism for the removal of the last barrier to viral release. Moreover, membrane fusion in this context appears to be mediated entirely by the phage-encoded spanins in a compartment devoid of ATP. Thus, the mechanism of membrane fusion can be addressed in a very simple system accessible to the power of phage genetics.

Author contributions: M.R. and R.Y. designed research; M.R., J.B., R.K., and J.C. performed research; R.Y. contributed new reagents/analytic tools; M.R., J.B., R.K., J.C., and R.Y. analyzed data; and M.R., J.B., and R.Y. wrote the paper.

The authors declare no conflict of interest.

This article is a PNAS Direct Submission.

[1]To whom correspondence should be addressed. Email: ryland@tamu.edu.

This article contains supporting information online at www.pnas.org/lookup/suppl/doi:10.1073/pnas.1420588112/-/DCSupplemental.

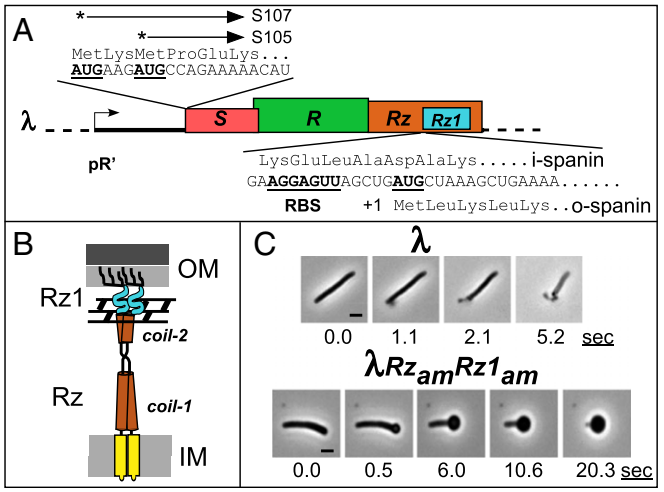

Fig. 1. (*A*) The lysis cassette of paradigm phage λ. The λ lysis genes encoding the holin (red), endolysin (green), i-spanin (brown), and o-spanin (cyan) are located downstream of the late gene promoter pR′. The λ *S* gene has a dual-start motif, encoding both the holin (S105) and antiholin (S107) (4). Both start codons are bold and underlined. The two-component spanin gene of λ is the representative of the embedded gene architecture. The insets show the translation frame of Rz1 in +1 frame of Rz. The strong ribosome binding site (RBS) for Rz1 translation is underlined. The start codon for Rz1 is bold and underlined. (*B*) Spanin topology. Cartoon models for the topology of the two-component spanin (Rz = i-spanin; Rz1 = o-spanin). The Rz i-spanin, embedded in the cytoplasmic membrane by an N-terminal TMD (yellow), has coiled-coil alpha helical periplasmic domains (brown) separated by a linker region. The mature Rz1 o-spanin (cyan) is attached to the OM via the three fatty acyl groups decorating the N-terminal Cys residue. Both the i-spanin and o-spanin form covalent homodimers linked by intermolecular disulfide bonds in the periplasmic domains (12). The i-spanin/o-spanin complex is shown connecting the IM and OM through the meshwork of the PG (black hatching). (*C*) Spanin-null lysis phenotype (reproduced from ref. 8). Representative time-series images of induced λ lysogens, either WT (*Top*) or $Rz_{am}Rz1_{am}$ (*Bottom*), are shown. Time (in seconds) is from first detectable change in cell morphology at the onset of the lysis process, ~50 min after induction. (Scale bar, 1 μm.)

Results

In Vitro Spheroplast Fusion by λ Spanins. To address how the spanin complex effected OM disruption, we were first stimulated by electron-microscopic images of the products of spanin-mediated lysis in the absence of holin function (Fig. S1) (2). In this case, endolysin activity was secreted directly to the periplasm by the host *sec* system, leaving the IM intact. In the absence of spanin function, endolysin-mediated degradation of the PG did not result in lysis. Instead, spherical cells were formed, bound by the OM. In the presence of spanins, however, lysis was observed and the lysis debris was dominated by highly vesicularized membranous structures (Fig. S1 *A*, *II* and *III*). This led us to posit that spanins achieve destruction of the OM by a topological solution: fusion of the IM and OM (Fig. 2*A*), analogous to the vesicular fusions central to Golgi trafficking, neurotransmitter release, and viral fusion (18).

To test this model, we developed a spheroplast fusion assay (Fig. 2*B*). First, we constructed two plasmids engineered to express either *Rz* or *Rz1* at physiological levels and also a fluorescent protein to label the spheroplast cytoplasm: GFP for *Rz* and mCherry for *Rz1*. The WT allele was used for the *Rz* construct, but for *Rz1*, a missense allele, *imRz1*, was constructed in which the parental Thr21–Ser22 codons were substituted by Asp codons. Asp residues in these positions, immediately distal to the lipoylated Cys, prevent mature lipoproteins, including Rz1, from being sorted to the OM by the host localization of lipoprotein (Lol) system (2, 19). We hypothesized that spheroplasting these cells by standard techniques (i.e., treatment with EDTA and lysozyme) (20) would expose the periplasmic domains of the Rz i-spanin and the ectopically localized imRz1 o-spanin. Mixtures of such spheroplasts should allow spanin complex formation between these exposed periplasmic domains, which, according to our model, would lead to fusing of the spheroplast membranes and mixing of the labeled cytoplasms (Fig. 2*B*). Accordingly, when the two induced cultures were mixed at a 1:1 ratio and converted to spheroplasts, we found ~10% of the product spheroplasts were labeled with both GFP and mCherry (Fig. 3 *B*, *II*). This meant that at least 20% of the input cell mixture participated in spheroplast fusion events, as each doubly labeled spheroplast required at least one input singly labeled cell. Most of the fusion events had occurred by the time of the first microscopic examination after spheroplasting (Fig. 3 *A* and *D*). However, occasionally, red- and green-labeled spheroplasts could be visualized in the process of fusion, which occurred only between spheroplasts already adhered together and was completed in the time range of 1–5 min (Fig. 3*C* and Movie S1). The double-labeled spheroplasts were larger and more irregular in shape than the spheroplasts with only a single label (Fig. 3*D*). No doubly labeled spheroplasts were produced when either plasmid was substituted with a vector lacking a spanin subunit (Fig. S2). However, fusion events were obtained, albeit at a much lower level, when both GFP and mCherry-labeled cells produced Rz (~3.5% doubly labeled spheroplasts) or imRz1 (~1% doubly labeled spheroplasts) (Fig. S3).

Lysis-Defective λ Spanins Fail to Fuse Spheroplasts in Vitro. By several criteria, in vitro spanin-mediated spheroplast fusion had similar properties to spanin-mediated OM disruption in vivo. First, spheroplast fusion was insensitive to the energization of the cytoplasmic membrane, as judged by the result that the presence of 10 mM potassium cyanide (KCN), shown in previous work to collapse the membrane potential and trigger holin function, had no effect on the yield of fused spheroplasts (Fig. S4). In addition, spheroplast fusion was sensitive to the allelic state of the spanin subunit. Three nonfunctional spanin missense alleles, all of which confer absolute lysis defects in vivo without affecting accumulation of the gene product (Fig. S5), were tested alone and in combination for fusion in vitro: I54N in Rz1, and R91P and Q151R in Rz (Fig. 3 *B*, *III*–*VI* and Fig. S2). Fusion was

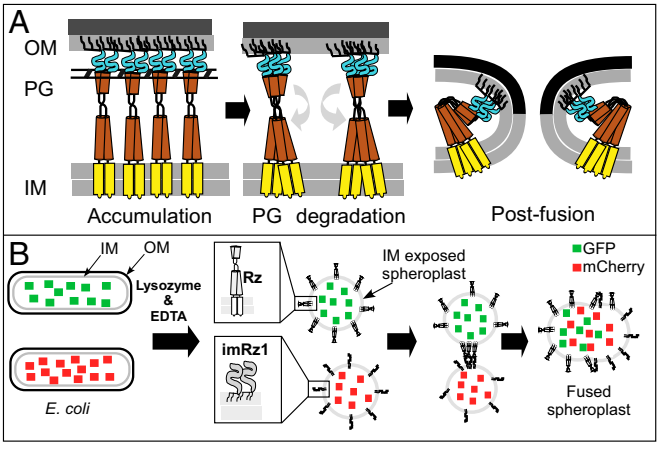

Fig. 2. (*A*) Membrane fusion model for Rz–Rz1 lytic function. During the infection cycle, spanin complexes connecting the IM and OM accumulate within the lacunae formed by PG cross-linking. Endolysin-mediated destruction of the PG liberates the spanins to oligomerize and undergo conformational changes to bring the opposing membranes into contact and stimulate IM–OM fusion. (*B*) Fusion assay. Shown are schematics of spheroplasts prepared from rod-shaped cells expressing either Rz/GFP (*Top*) or imRz1/mCherry (*Bottom*). Spanin-mediated fusion events result in mixed cytoplasmic contents, labeled with both GFP and mCherry.

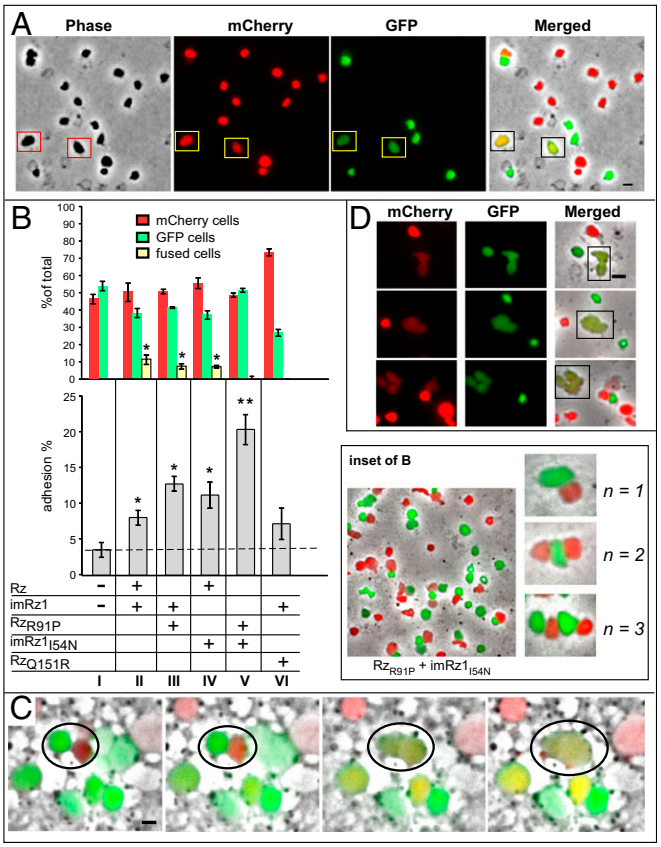

Fig. 3. (*A*) Fluorescence images of the fused spheroplasts (boxes) indicate the colocalization of the GFP and mCherry. (*B*) Quantification of fusion events. (*Upper*) The percentage of labeled spheroplasts obtained with different combinations of *Rz* and *imRz1* alleles labeled at the bottom. Green bar, spheroplasts labeled with GFP; red bar, spheroplasts labeled with mCherry; yellow bar, spheroplasts labeled with both fluorescent proteins. (*Middle*) The percentage of spheroplast–spheroplast adhesions (*Experimental Procedures* and *Inset* of *B*). The adhesion fraction increases to ∼24% when the fusion is blocked by mutations in both the Rz and Rz1 periplasmic domains (see *Experimental Procedures* and *Inset* of *B*). The dashed line represents the background level of adhesions in the absence of spanin protein. Values indicate the mean ± SD of three replicates (*I–V*) and two replicates (*VI*). Spheroplast count; $n = 533 \pm 23$ for each replicate. $^{*}P < 0.05$; $^{**}P < 0.005$ versus negative control (one-tailed *t* test). (*C*) Snapshot of spheroplast fusion caught in action. Circle marks two differentially labeled cells that undergo fusion; time between first and last images was <60 s. (*D*) A collage of representative images of fused spheroplasts (boxed) that are larger in size and more irregular in shape. (Scale bar, 5 μm.)

not affected by the introduction of either I54N into *imRz1* or R91P into *Rz*, suggesting that the fusion of cytoplasmic membranes in vitro is less demanding than the fusion of the IM and OM in vivo. Nevertheless, when both missense changes were present, fusion was abolished (Fig. S2 and Fig. 3*B*, compare *V* with *III* and *IV*). Although fusion was not detected with this combination of alleles, there was an increase in spheroplast adhesion, defined as the number of visible interfaces between differentially labeled spheroplasts (Fig. 3 *B*, *Inset*). Indeed, in the double mutant experiment, spheroplast adhesions were elevated compared with others (Fig. 3 *B*, *Lower*, compare *V* with the rest). This suggests that the mutant I54N o-spanin and R91P i-spanin subunits retained the ability to form a complex but were blocked in the actual membrane fusion step. Interestingly, spheroplast adhesion was also elevated when Rz was surface exposed from both types of cells (Fig. S3). This is likely due to the ability of the periplasmic domain of Rz to form coiled-coil bundles (13). When we tested another i-spanin allele, Rz_{Q151R}, we found that fusion was abolished irrespective of the allelic state of *imRz1* (Fig. 3*B*, compare *VI* with the rest). With this *Rz* allele, persistence of adhesions could not be reliably assessed because the number of surviving GFP-labeled spheroplasts was significantly reduced, suggesting that the Q151R substitution at the extreme C terminus of Rz is detrimental to the membrane. In any case, taken together, these results support the notion that the spanin complex is membrane-fusogenic, consistent with our model that the last step in the lysis pathway is spanin-mediated fusion between the IM and OM.

The PG Meshwork Inhibits Spanin Lytic Function. Because the spanin complexes form throughout the morphogenesis phase of the λ infection cycle, there must be some regulation that prevents premature membrane fusion, which would obviously destroy the integrity of the cytoplasmic membrane. The intact PG is a meshwork of glycosidic chains cross-linked by oligopeptides, forming covalent lacunae of ∼2 nm in radius (21). The simplest notion is that during the infection cycle, each spanin complex connecting the IM and OM is restricted to the lacuna of the intact PG within which it is formed (Fig. 2 *A*, *Accumulation* panel, black hatching) and thus prevented from lateral diffusion. Liberation of these complexes by endolysin-mediated degradation of the cell wall would permit oligomerization of the complexes, which we have suggested to be the source of the free energy needed for membrane fusion (Fig. 2 *A*, *PG Degradation* panel). To test the idea that it is the meshwork of the PG that blocks spanin function, we examined spanin-mediated lysis in conditions where the murein was depleted in an endolysin-independent fashion. To deplete the level of PG, we used an *Escherichia coli dadX alr* strain. The *dadX* and *alr* genes encode the alanine racemases necessary for conversion of L-Ala to D-Ala, which is essential for the biosynthesis of PG (22–24). Removal of D-Ala from the medium blocks net PG synthesis and causes the growing auxotrophic cells to gradually lose their rod-like morphology (Fig. S6; also see Fig. 4 *A*, *Inset*), starting with a localized bulging phenotype similar to cells treated with β-lactam antibiotics or vancomycin (25, 26). To prevent endolysin function, we constructed a λS_{am} lysogen of this strain. The S_{am}-null holin allele blocks endolysin function by restricting the muralytic enzyme to the cytoplasm but has no effect on the expression of the spanin genes or spanin complex formation (2). When we induced this lysogen after starving for D-Ala, dramatic lysis of the spherical cells was observed beginning ∼15 min after induction (Fig. 4*A*, filled squares). This lysis required both the i-spanin Rz (Fig. 4*A*, open squares) and the o-spanin Rz1 (Fig. 4*A*, open triangles) and was blocked by readdition of D-Ala (Fig. 4*A*, open circles) at the time of induction. By comparison, lysis was not observed in cells prototrophic for D-Ala (Fig. 4*A*, filled triangles and crosses). In another experiment, at the time of induction, we abruptly depleted D-Ala from the culture (Fig. 4*B*). Under these acute conditions, in the absence of spanin function, the cells undergo morphological changes characteristic of cell wall defects (Fig. 4 *C*, *Upper* panels) and some eventually lyse beginning at ∼100–110 min (Fig. 4*B*, open squares). In contrast, in the presence of the functional spanins, lysis occurs much earlier, at ∼45–50 min, and more rapidly (Fig. 4*B*, filled squares). Importantly, many of the lysed cells retained their rod-shaped morphology, suggesting that the spanin-mediated lysis occurred even before the murein was sufficiently depleted to cause gross morphological changes (Fig. 4 *C*, *Lower* panels). These experiments support the notion that the PG network acts as a negative regulator of spanin lytic function.

Discussion

Membrane Fusion as the Last Step in Lysis. Here we have presented results that phage spanins can mediate efficient membrane fusion in spheroplasts. Moreover, spheroplast fusion by the Rz–Rz1 system of λ is blocked by missense mutations that also block the last step of λ lysis, without affecting accumulation of the spanin subunits. These results strongly support the model that the last step in

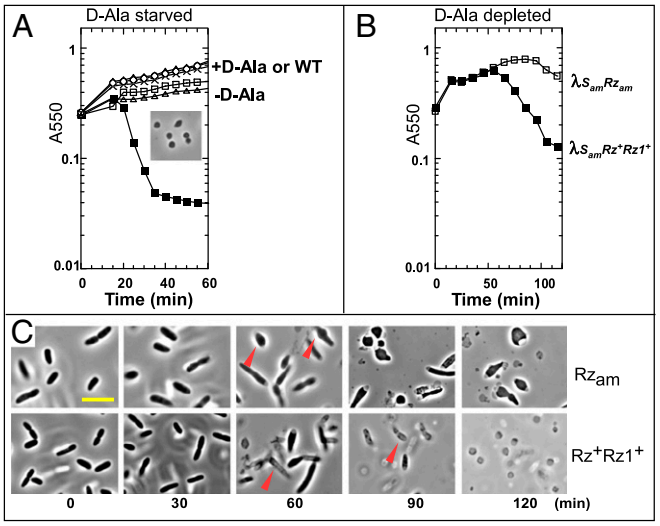

Fig. 4. Spanin function is negatively regulated by the PG. (*A*) Cells lysogenic for λS_{am} Rz^+Rz1^+ and auxotrophic for D-Ala were grown in LB in the absence of D-Ala, induced at t = 0, and monitored for culture mass (A_{550}). The induced culture underwent sudden lysis beginning at t = ∼15 min (filled squares). This lysis was blocked in the WT host (D-Ala prototroph; filled triangles) or in the D-Ala auxotroph supplemented with 150 μM D-Ala (open circles). Lysis was also blocked in the starved auxotrophs if either *Rz* (open squares) or *Rz1* (open triangles) was absent. In these conditions, the cells maintained their spherical morphology (see *Inset* for image of Rz^- cells; $Rz1^-$ cells were identical). (*B*) D-Ala auxotrophic cells lysogenic for λS_{am} were induced and suddenly depleted of D-Ala at time = 0 (*Experimental Procedures*). Onset of lysis was observed ∼60 min after induction of $\lambda S_{am}Rz^+$ $Rz1^+$ (filled squares), whereas only a slight decrease in A_{550} was observed for the isogenic Rz_{am} prophage (open squares). (*C*) Morphology of cells from the experiment of *B* was imaged by phase-contrast microscopy at indicated sampling times after induction. Arrowheads indicate swollen morphology of the D-Ala–deprived cells in the top images and rod-shaped cells that have undergone lysis in the bottom images. [Scale bar (yellow), 5 μm.]

lysis of Gram-negative hosts is topological rather than degradative (2, 27). In other words, the final barrier to phage progeny release, the OM, is circumvented through fusion with the IM.

In addition, the experiments with the D-Ala prototroph indicate that the spanin-mediated lytic step, which we suggest is IM–OM fusion, is not directly coupled to any other phage lytic function, including endolysin-mediated degradation of the cell wall. Instead, the spanin complexes can cause fusion upon partial depletion of the PG imposed by starvation for D-Ala, even when the PG is sufficiently intact to preserve the rod-shaped cell morphology. These results support our interpretation of the dramatic "local blowout" morphology characteristic of λ lysis (8). We have suggested that endolysin molecules escaping through the μm-scale IM holes formed by the triggered holin population initially degrade the patch of the PG over the hole. This interpretation is based on the observation that, in the absence of spanin function, the envelope deforms beginning at a confined point and is then transformed into a spherical shape by progressive deformation along the long axis of the cell, presumably reflecting diffusion of the muralytic endolysin molecules away from the initial hole. Thus, the lytic blowout occurs when sufficient spanin complexes are liberated within the degraded area of the PG.

Mechanism of Membrane Fusion. The results presented here allow inferences to be drawn about the mechanism of IM–OM fusion. First, the fact that *Rz–Rz1* mutations that block lysis also block fusion in vitro without affecting accumulation or subcellular localization of the spanin subunits suggests that the in vitro spheroplast fusion and the IM–OM fusion are mechanistically similar, if not identical. In particular, the combination of the Rz_{R91P} i-spanin and $Rz1_{I54N}$ o-spanin alleles, despite having no effect on accumulation, not only blocks both lysis and spheroplast fusion but also results in the accumulation of adhered spheroplasts. This suggests that these alleles are defective in a final step in membrane fusion, beyond bringing the target membranes into contact. Indeed, studies of other membrane fusion systems have suggested that, after the bilayers are brought together by a protein complex, one or both of the opposed leaflets must be perturbed to initiate the fusion event (18, 28, 29). In general, opposing membranes are brought into close proximity, often by a protein with propensity to form coiled-coil structures. For example, in Golgi vesicular fusion, SNARE proteins anchored in both membranes undergo coiled-coil interactions that bring the bilayers into apposition (30, 31). Moreover, in some fusion systems, a protein domain with the intrinsic ability to destabilize a membrane leaflet is required; for example, the fusion peptide p15 of orthorheovirus has a polyproline helix shown to be essential for viral entry (32). The spanin system has features reminiscent of both these examples, in that the i-spanin Rz has conserved coiled-coil helical domains that occupy nearly all of the soluble segment. As noted previously by Bryl et al. (17), the mature o-spanin Rz1 has 25% proline content, including a conserved run of five proline residues, which could confer membrane-destabilizing character. Indeed, the lower level of fusion detected in the homotypic situations (i.e., with Rz or imRz1 in both cells; Fig. S3) suggests that both proteins have some fusogenic character. This observation suggests an attractive rationale for the evolution of the two-component spanins in which ancestral phages of Gram-negative hosts had less efficient primordial versions of either the i-spanin or the o-spanin; a phage that acquired both might have a significant fitness advantage, after which evolutionary pressure might result in the interaction of the two subunits and the clustering of their genes.

Despite these functional homologies, the fact that in the case of the Rz_{I54N} and $Rz1_{R91P}$ lysis-defective alleles each retains undiminished spheroplast fusion activity but exhibits a synthetic defect (i.e., the presence of both blocks fusion) suggests that IM–OM fusion is more demanding than IM–IM fusion. This is not surprising considering our previous finding that in the absence of the PG the OM is capable of withstanding the internal osmotic pressure of the cell (8). This conclusion has been recently confirmed by other approaches (26). Thus, the OM has significantly more tensile strength than the IM, which is rapidly destroyed in conditions of osmotic imbalance (20, 33).

Energetics of Spanin Function. Because spanin-mediated fusion occurs in the context of the periplasm, where nucleotide phosphate energy carriers are not available, it is of interest to consider the source of the free energy for spanin-mediated membrane fusion. Although the i-spanin has a transmembrane domain (TMD) that spans the IM and thus possesses a cytoplasmic N terminus, the cytoplasmic domain is not large enough to be involved directly in ATP interactions. Another potential source of energy is the membrane potential, which is ∼0.2 V in *E. coli* under standard conditions (34). However, spanins have been shown to function normally not only after holin triggering, which collapses the membrane potential (3), but also in the absence of holin function under conditions where the PG is degraded by a secreted endolysin (2). In the latter case, the energized state of the cytoplasmic membrane is undisturbed. The result reported here, showing that cyanide had no effect on the spanin-mediated spheroplast fusion, is consistent with that finding. By extension, because the energization of the IM is irrelevant to spanin function, so is energy transduction from the IM to the OM via the TonB-dependent and TolQ-dependent pathways (35). We favor the notion that the free energy for fusion results from conformational changes at the secondary, tertiary, and quaternary levels after liberation of the spanins from the entrapping meshwork of the PG. Dramatic increases in

Table 1. Strains, phages, and plasmids

Strains	Genotypes and relevant features	Sources
Bacteriophages		
λ900	λ*Δ(stf tfa)::cat* cI_{857} *bor::kan;* carries Cam^R and Kan^R; Rz^+Rz1^+	Laboratory stock
λ901	λ900 S_{am7} nonsense allele of *S* holin gene	Laboratory stock
λ901Rz_{Q100am} $Rz1^+$		(2)
λ901Rz^+Rz1_{W38am}		(2)
λ901Rz_{Q100am} $Rz1_{W38am}$		(2)
E. coli strains		
MC1000	$araD_{139}$ $\Delta(ara\text{-}leu)_{7679}$ *galU galK* Δ *lac*	(23)
MB2159	MC1000 $dadX_{EC}$*::frt* alr_{EC}*::frt*	(23)
MC1000 (λ901)	Lysogen carrying λ901prophage	This study
MC1000 (λ901$Rz_{Q100am}Rz1_{W38am}$)		This study
MB2159 (λ901)		This study
MB2159 (λ901Rz_{Q100am} $Rz1^+$)		This study
MB2159 (λ901Rz^+Rz1_{W38am})		This study
MB2159 (λ901Rz_{Q100am} $Rz1_{W38am}$)		This study
RY17299 $lacI^{q1}$	Derived from MG1655Δ *tonA*	(38)
Plasmids		
pQ	λ *Q* cloned under $P_{lac/ara\text{-}1}$ promoter in a low copy number plasmid pZS-24*	(39)
pRE	Medium copy vector carrying Q-dependent pR′ (λ late promoter)	(38)
pRz	*Rz* cloned in pRE with $Rz1W_{38am}$ null mutation	(2)
pimRz1	$Rz1_{T21DS22D}$ cloned in pRE	(2)
pRz/ GFP	*gfp* cloned downstream of *Rz* in pRz	This study
pimRz1/GFP	*gfp* cloned downstream of imRz1 in pRz	This study
pRz_{R91P}/GFP	pRz/GFP carrying R91P allele of *Rz*	This study
pRz_{Q151R}/GFP	pRz/GFP carrying Q151R allele of *Rz*	This study
pmCherry/ $imRz1_{I54N}$	pmCherry/imRz1 carrying I54N allele of *imRz1*	This study
$pGFP_{A206K}$	*gfp* cloned downstream of the pR′ promoter	Laboratory stock
pmCherry	*mCherry* cloned downstream of the pR′ promoter	Laboratory stock

complex size and alpha-helical content have been demonstrated for the formation of equimolar complexes of sRz and sRz1, the purified soluble periplasmic domains of the i-spanin and o-spanin subunits (13).

Next Steps. There is immense diversity among spanins, including two-component spanin genes that have different genetic architectures from the embedded structure of lambda *Rz–Rz1* (Fig. 1*A* and Fig. S7) (14). The massive evolutionary diversity should empower bioinformatic analysis once domains can be tentatively assigned to functions in the membrane fusion pathway and, potentially, will permit domain-interaction analysis through the construction of hybrid spanins. Combined with the facile genetics of λ and phage in general, the spanin system should provide a powerful platform for dissecting the molecular basis of membrane fusion. In addition, some phages of Gram-negative hosts, instead of having an i-spanin/o-spanin gene pair, encode a unimolecular spanin (u-spanin) that effects OM disruption during lysis (Fig. S7) (14). The prototype u-spanin is gp*11* of the paradigm phage T1. Gp11 has an OM lipoprotein signal at the N terminus and a C-terminal domain that spans the IM (Fig. S7, *Inset*). The periplasmic domain of gp*11* lacks the characteristic features of the two-component spanins, including intermolecular disulfide bonds and predicted coiled-coil helical structure (12, 13), and is instead predicted to be dominated by β-strand structures (14). In work to be described elsewhere, gp*11* has also been shown to promote spheroplast fusion, which should allow comparative genetic and biochemical studies to focus on the molecular features essential for membrane fusion.

Experimental Procedures

Bacterial Growth, Induction, and Time-Lapse Phase-Contrast Microscopy. Bacterial strains used in this study are listed in Table 1. Bacteria were grown in standard LB media or on LB agar, supplemented with appropriate antibiotics, as indicated: ampicillin (Amp, 100 μg/mL), kanamycin (Kan, 40 μg/mL), and chloramphenicol (Cam, 10 μg/mL). D-Ala auxotrophic strains were supplemented with 150 μM of D-Ala as indicated. Cultures were started with a 1:300 dilution of a fresh overnight culture in 25 mL of media in a 250 mL flask and grown with aeration either at 30 °C for lysogenic cultures or at 37 °C for nonlysogens. Lysogens were thermally induced at $A_{550} \sim 0.25$ by shifting to 42 °C for 15 min and then continued growth at 37 °C until lysis. Cultures induced for the fusion assay (see *Spheroplast Fusion Assay and Fluorescence Microscopy* below) were chemically induced by adding isopropyl β-D-thiogalactopyranoside (IPTG) to a final concentration of 1 mM. Phase-contrast microscopy was conducted as described previously (8), except that an EC Plan-Neofluor 100×/1.3 oil Ph3/∞/0.17 objective was used to capture the images. For imaging, a 1 mL sample of growing culture was harvested by centrifugation at 9,500 × *g* for 1 min and immediately resuspended in 100 μL of LB, of which 1 μL was spotted on the ethanol-washed glass slide and covered with the 22 × 22 mm coverslip before mounting on the stage for the inverted microscope objective. Cells of growing cultures were imaged every 30 min or as indicated.

D-Ala Starvation/Depletion. To impose D-Ala starvation, an overnight culture grown in supplemented D-Ala was washed twice with plain LB before a 1:300 dilution into 25 mL of LB amended to 10% (wt/vol) sucrose. For D-Ala depletion experiments, the overnight culture diluted 1:300 into fresh LB media and 150 μM D-Ala. At $A_{550} \sim 0.25$, the culture was harvested by centrifugation at 6,500 × *g* for 5 min at room temperature using a Thermo Scientific F15S-8 × 50cy rotor, washed three times with LB to remove the remaining D-Ala in the media, and resuspended in fresh media (without sucrose).

Strain and Plasmid Construction. Strain MB2159, carrying complete deletions of *alr* and *dadX*, and its isogenic parental MC1000 were generous gifts from Michael Benedik (Texas A&M University, College Station, TX) (23). Both of these strains were lysogenized with phage λ901, λ901$Rz_{Q100\ am}$ $Rz1^+$, λ901Rz^+ $Rz1_{w38am}$ or λ901$Rz_{Q100\ am}$ $Rz1_{w38am}$ (Table 1) as described elsewhere (36). Phage λ901 and its derivatives carry the temperature-sensitive repressor *cI857* and contain deletion substitutions of nonessential genes, *stf::cam* and *bor::kan*. Lysogens were thus selected by plating on LB-kan plus D-Ala whenever necessary. Candidate lysogens were tested for a single copy prophage as described elsewhere (37).

The plasmids used in this study were constructed by standard molecular biology techniques. The plasmid of pBR322 derivative engineered with a λ

MICROBIOLOGY

late promoter pR′ was used to regulate the expression of *Rz*, *imRz1*, *GFP*, and *mCherry*. In the paired clone, *GFP* and *Rz* and *mCherry* and *imRz1* were cloned 30 and 22 nucleotides apart with their own Shine–Dalgarno sequence for translation. The expression of all individual or paired clones was dependent on the activity of the antiterminator Q of λ. In a nonlysogenic strain, the antiterminator Q was supplied in trans from a plasmid pQ, a low-copy plasmid with a IPTG-inducible $P_{lac/ara-1}$ promoter (2).

Spheroplast Fusion Assay and Fluorescence Microscopy. The host for all spheroplast experiments was RY17299, which is MG1655 *lacI*^{q1} *tonA::*Tn*10* (Table 1). This host was transformed with pQ, a low copy plasmid carrying the λ *Q* late activator gene under *lac* control. The plasmid pQ is compatible with the plasmids carrying the spanin genes (*Rz* and *imRz1*) and fluorescent protein genes (*gfp* and *mCherry*) (see plasmid construction above) cloned under the control of the λ late promoter, pR′.

For Rz–imRz1 fusion experiments, logarithmically growing cells were induced at $A_{550} \sim 0.25$. At t = 55 min, the cultures were placed on ice for 10 min to stop growth. Approximately 26 ± 1 A_{550} units of cells from each culture were harvested by centrifugation at 6,500 × *g* for 10 min at 4 °C using a Thermo Scientific F15S-8 × 50cy rotor. Pellets were resuspended, washed twice in cold high sucrose buffer (0.75 M sucrose, 10 mM Tris·acetate, and pH 7.8), and finally resuspended in 0.5 mL high sucrose buffer. The concentrated cells from two cultures (e.g., one expressing GFP and Rz and another expressing mCherry and imRz1) were combined to make 1 mL final volume and transferred into a small glass beaker on ice. This mixture was first supplemented with 10 μL of 5 mg/mL DNase (Sigma-Aldrich) and 50 μL of 10 mg/mL egg-white lysozyme (0.1 mg/10 A_{550} units; Sigma-Aldrich) with gentle mixing, followed by incubation in ice for 2–4 min. For spheroplasting, the lysozyme-treated cells were then treated with 2.1 mL of 1.15 mM EDTA (twice the volume of initial resuspension) by slow swirling in ice bath as described elsewhere (20). The EDTA treatment was adjusted to a flow rate of ∼250 μL/min. All preparation steps were carefully done in ice after harvesting the cells. We have noticed that the treatment of cells with higher amounts of lysozyme caused spheroplast clumping, an effect that has been described elsewhere (20). We also noticed that spheroplasting of cells above $A_{550} \sim 0.3$ was generally unsuccessful. After ∼10 min incubation of the spheroplast mixture in ice, 1 μL of sample was placed onto a coverslip (24 × 50 mm; thickness, 0.16 mm), gently covered with a premade agarose pad (0.6% wt/vol in 0.75 M sucrose) of ∼5 × 5 mm dimensions, and immediately imaged by an inverted epifluorescence microscope (Eclipse TE2000-E; Nikon) using a 100× objective (Plan Fluor, numerical aperture, 1.40; oil immersion) and standard filter sets. Microscopy was done at room temperature. Images were acquired using a CCD camera (Cascade512; Photometrics). Image analysis was done using NIS-Elements imaging software. For each experiment, snapshots of 10–20 different frames were captured before repeating the process. Each frame was analyzed individually, and the number of spheroplasts emitting red, green, or both were manually scored. The percentage of fused spheroplast was calculated using the basic formula [% = (number of fused cells / total) * 100; total = red + green + both]. Similarly, % of adhesion point = (*n* / total) * 100, where *n* is the number of visible interface between red and green as shown in Fig. 3 *B*, *Inset*. For example, if a single red cell is clustered with two green cells, then *n* = 2 and the total cell number is 3.

ACKNOWLEDGMENTS. We thank Dr. Michael Benedik of the Department of Biology at Texas A&M University for providing us with the racemase mutant strains. We also thank Dr. Lanying Zhang and her group for help and access to their fluorescence microscope. The clerical assistance of Daisy Wilbert is highly appreciated. This work was supported by Public Health Service Grant GM27099 and by the Center for Phage Technology at Texas A&M University, jointly sponsored by Texas AgriLife.

1. Young R, Wang IN (2006) Phage lysis. *The Bacteriophages*, ed Calendar R (Oxford Univ Press, Oxford), 2nd Ed, pp 104–126.
2. Berry J, Summer EJ, Struck DK, Young R (2008) The final step in the phage infection cycle: The Rz and Rz1 lysis proteins link the inner and outer membranes. *Mol Microbiol* 70(2):341–351.
3. White R, et al. (2011) Holin triggering in real time. *Proc Natl Acad Sci USA* 108(2): 798–803.
4. Bläsi U, Chang CY, Zagotta MT, Nam KB, Young R (1990) The lethal λ *S* gene encodes its own inhibitor. *EMBO J* 9(4):981–989.
5. Wang IN, Smith DL, Young R (2000) Holins: The protein clocks of bacteriophage infections. *Annu Rev Microbiol* 54:799–825.
6. Young R (1992) Bacteriophage lysis: Mechanism and regulation. *Microbiol Rev* 56(3): 430–481.
7. Wang I-N, Deaton J, Young R (2003) Sizing the holin lesion with an endolysin-β-galactosidase fusion. *J Bacteriol* 185(3):779–787.
8. Berry J, Rajaure M, Pang T, Young R (2012) The spanin complex is essential for lambda lysis. *J Bacteriol* 194(20):5667–5674.
9. Hanych B, Kedzierska S, Walderich B, Uznański B, Taylor A (1993) Expression of the Rz gene and the overlapping Rz1 reading frame present at the right end of the bacteriophage lambda genome. *Gene* 129(1):1–8.
10. Kedzierska S, Wawrzynów A, Taylor A (1996) The Rz1 gene product of bacteriophage lambda is a lipoprotein localized in the outer membrane of Escherichia coli. *Gene* 168(1):1–8.
11. Taylor A, Kedzierska S, Wawrzynów A (1996) Bacteriophage lambda lysis gene product modified and inserted into Escherichia coli outer membrane: Rz1 lipoprotein. *Microb Drug Resist* 2(1):147–153.
12. Berry JD, Rajaure M, Young R (2013) Spanin function requires subunit homodimerization through intermolecular disulfide bonds. *Mol Microbiol* 88(1):35–47.
13. Berry J, Savva C, Holzenburg A, Young R (2010) The lambda spanin components Rz and Rz1 undergo tertiary and quaternary rearrangements upon complex formation. *Protein Sci* 19(10):1967–1977.
14. Summer EJ, et al. (2007) *Rz*/*Rz1* lysis gene equivalents in phages of Gram-negative hosts. *J Mol Biol* 373(5):1098–1112.
15. Bartel PL, Roecklein JA, SenGupta D, Fields S (1996) A protein linkage map of *Escherichia coli* bacteriophage T7. *Nat Genet* 12(1):72–77.
16. Krupovič M, Cvirkaitė-Krupovic V, Bamford DH (2008) Identification and functional analysis of the *Rz*/*Rz1*-like accessory lysis genes in the membrane-containing bacteriophage PRD1. *Mol Microbiol* 68(2):492–503.
17. Bryl K, Kedzierska S, Laskowska M, Taylor A (2000) Membrane fusion by proline-rich Rz1 lipoprotein, the bacteriophage lambda Rz1 gene product. *Eur J Biochem* 267(3): 794–799.
18. Jahn R, Lang T, Südhof TC (2003) Membrane fusion. *Cell* 112(4):519–533.
19. Yamaguchi K, Yu F, Inouye M (1988) A single amino acid determinant of the membrane localization of lipoproteins in *E. coli*. *Cell* 53(3):423–432.
20. Osborn MJ, Munson R (1974) Separation of the inner (cytoplasmic) and outer membranes of Gram-negative bacteria. *Methods Enzymol* 31(A):642–653.
21. Demchick P, Koch AL (1996) The permeability of the wall fabric of *Escherichia coli* and *Bacillus subtilis*. *J Bacteriol* 178(3):768–773.
22. Glauner B, Höltje JV, Schwarz U (1988) The composition of the murein of *Escherichia coli*. *J Biol Chem* 263(21):10088–10095.
23. Strych U, Penland RL, Jimenez M, Krause KL, Benedik MJ (2001) Characterization of the alanine racemases from two mycobacteria. *FEMS Microbiol Lett* 196(2):93–98.
24. Strych U, Benedik MJ (2002) Mutant analysis shows that alanine racemases from *Pseudomonas aeruginosa* and *Escherichia coli* are dimeric. *J Bacteriol* 184(15): 4321–4325.
25. Huang KC, Mukhopadhyay R, Wen B, Gitai Z, Wingreen NS (2008) Cell shape and cell-wall organization in Gram-negative bacteria. *Proc Natl Acad Sci USA* 105(49): 19282–19287.
26. Yao Z, Kahne D, Kishony R (2012) Distinct single-cell morphological dynamics under beta-lactam antibiotics. *Mol Cell* 48(5):705–712.
27. Young R (2014) Phage lysis: Three steps, three choices, one outcome. *J Microbiol* 52(3):243–258.
28. Chernomordik LV, Kozlov MM (2008) Mechanics of membrane fusion. *Nat Struct Mol Biol* 15(7):675–683.
29. Harrison SC (2008) Viral membrane fusion. *Nat Struct Mol Biol* 15(7):690–698.
30. Rothman JE, Wieland FT (1996) Protein sorting by transport vesicles. *Science* 272(5259):227–234.
31. Weber T, et al. (1998) SNAREpins: Minimal machinery for membrane fusion. *Cell* 92(6): 759–772.
32. Top D, Read JA, Dawe SJ, Syvitski RT, Duncan R (2012) Cell-cell membrane fusion induced by p15 fusion-associated small transmembrane (FAST) protein requires a novel fusion peptide motif containing a myristoylated polyproline type II helix. *J Biol Chem* 287(5):3403–3414.
33. Birdsell DC, Cota-Robles EH (1967) Production and ultrastructure of lysozyme and ethylenediaminetetraacetate-lysozyme spheroplasts of *Escherichia coli*. *J Bacteriol* 93(1):427–437.
34. Felle H, Porter JS, Slayman CL, Kaback HR (1980) Quantitative measurements of membrane potential in *Escherichia coli*. *Biochemistry* 19(15):3585–3590.
35. Braun V, Endriss F (2007) Energy-coupled outer membrane transport proteins and regulatory proteins. *Biometals* 20(3-4):219–231.
36. Zhang N, Young R (1999) Complementation and characterization of the nested *Rz* and *Rz1* reading frames in the genome of bacteriophage lambda. *Mol Gen Genet* 262(4-5):659–667.
37. Powell BS, Rivas MP, Court DL, Nakamura Y, Turnbough CL, Jr (1994) Rapid confirmation of single copy lambda prophage integration by PCR. *Nucleic Acids Res* 22(25): 5765–5766.
38. Park T, Struck DK, Deaton JF, Young R (2006) Topological dynamics of holins in programmed bacterial lysis. *Proc Natl Acad Sci USA* 103(52):19713–19718.
39. Gründling A, Manson MD, Young R (2001) Holins kill without warning. *Proc Natl Acad Sci USA* 98(16):9348–9352.